Understanding stellar activity-induced radial velocity jitter using simultaneous K2 photometry and HARPS RV measurements

M. Oshagh, N. C. Santos, P. Figueira, S. C. C. Barros, J. -f. Donati, V. Adibekyan, J. P. Faria, C. A. Watson, H. M. Cegla, X. Dumusque, et al.

A&A 606, A107 (2017)
DOI: 10.1051/0004-6361/201731139

Astronomy & Astrophysics

Understanding stellar activity-induced radial velocity jitter using simultaneous *K2* photometry and HARPS RV measurements⋆

M. Oshagh[1,2], N. C. Santos[2,3], P. Figueira[2], S. C. C. Barros[2], J.-F. Donati[4,5], V. Adibekyan[2], J. P. Faria[2,3], C. A. Watson[6], H. M. Cegla[6,7,8], X. Dumusque[7], E. Hébrard[9], O. Demangeon[2], S. Dreizler[1], I. Boisse[10], M. Deleuil[10], X. Bonfils[11], F. Pepe[7], and S. Udry[7]

[1] Institut für Astrophysik, Georg-August Universität Göttingen, Friedrich-Hund-Platz 1, 37077 Göttingen, Germany
e-mail: moshagh@astro.physik.uni-goettingen.de
[2] Instituto de Astrofísica e Ciências do Espaço, Universidade do Porto, CAUP, Rua das Estrelas, 4150-762 Porto, Portugal
[3] Departamento de Física e Astronomia, Faculdade de Ciências, Universidade do Porto, Rua do Campo Alegre, 4169-007 Porto, Portugal
[4] Université de Toulouse, UPS-OMP, IRAP, 14 avenue E. Belin, 31400 Toulouse, France
[5] CNRS, IRAP/UMR 5277, 14 avenue E. Belin, 31400 Toulouse, France
[6] Astrophysics Research Centre, School of Mathematics & Physics, Queen's University Belfast, University Road, Belfast, BT7 1NN, UK
[7] Observatoire de Genève, Université de Genève, 51 chemin des Maillettes, 1290 Versoix, Switzerland
[8] Swiss National Science Foundation NCCR-PlanetS CHEOPS Fellow, 3012 Bern, Switzerland
[9] Department of Physics and Astronomy, York University, Toronto, ON M3J 1P3, Canada
[10] Aix-Marseille Université, CNRS, LAM (Laboratoire d'Astrophysique de Marseille) UMR 7326, 13388 Marseille, France
[11] UJF-Grenoble 1/CNRS-INSU, Institut de Planétologie et d'Astrophysique de Grenoble (IPAG) UMR 5274, 38041 Grenoble, France

Received 9 May 2017 / Accepted 5 July 2017

ABSTRACT

One of the best ways to improve our understanding of the stellar activity-induced signal in radial velocity (RV) measurements is through simultaneous high-precision photometric and RV observations. This is of prime importance to mitigate the RV signal induced by stellar activity and therefore unveil the presence of low-mass exoplanets. The *K2* Campaign 7 and 8 fields of view were located in the southern hemisphere, and provided a unique opportunity to gather unprecedented simultaneous high-precision photometric observation with *K2* and high-precision RV measurements with the HARPS spectrograph to study the relationship between photometric variability and RV jitter. We observed nine stars with different levels of activity, from quiet to very active. We first probed the presence of any meaningful relation between measured RV jitter and the simultaneous photometric variation, and also other activity indicators (such as BIS, FWHM, $\log R'_{\rm HK}$, and F8) by evaluating the strength and significance of the monotonic correlation between RVs and each indicator. We found that for the case of very active stars, strong and significant correlations exist between almost all the observables and measured RVs; however, when we move towards lower activity levels the correlations become random, and we could not reach any conclusion regarding the tendency of correlations depending on the stellar activity level. Except for the F8 whose strong correlation with RV jitter persists over a wide range of stellar activity level, and thus our result suggests that F8 might be a powerful proxy for activity-induced RV jitter over a wide range of stellar activity. Moreover, we examine the capability of two state-of-the-art modeling techniques, namely the *FF′* method and *SOAP2.0*, to accurately predict the RV jitter amplitude using the simultaneous photometric observation. We found that for the very active stars both techniques can predict the amplitude of the RV jitter reasonably well; however, at lower activity levels the *FF′* method underpredicts the RV jitter amplitude.

Key words. methods: data analysis – stars: activity – techniques: radial velocities – techniques: photometric – methods: numerical

1. Introduction

It is well-known that the presence of stellar active regions (such as star spots or plages) on a rotating star can generate astrophysical noise in high-precision photometric and radial velocity (RV) time series. The activity-induced RV jitter can hamper the detection of low-mass planets, complicate the confirmation of transiting planets, and may even mimic a planetary signal (e.g., Queloz et al. 2001; Santos et al. 2002; Huélamo et al. 2008; Figueira et al. 2010; Santos et al. 2010; Boisse et al. 2011; Dumusque et al. 2011; Santos et al. 2014; Robertson et al. 2014; Díaz et al. 2016). In photometric observations the activity noise may also cause severe difficulties in accurately characterizing transiting planets through transit light-curves analysis (e.g., Czesla et al. 2009; Oshagh et al. 2013, 2014; Barros et al. 2014; Oshagh et al. 2015).

Many studies have suggested that there is a correlation between the amplitude of photometric variability of stars and the amplitude of RV jitter. For instance, the classic work by Saar et al. (1998) established the first estimate of this correlation,

⋆ RV measurements obtained from the HARPS pipeline are only available in electronic form at the CDS via anonymous ftp to cdsarc.u-strasbg.fr (130.79.128.5) or via http://cdsarc.u-strasbg.fr/viz-bin/qcat?J/A+A/606/A107

Table 1. Main stellar parameters, the EPIC number, the number of *K2* campaign, and number of HARPS RV observations of our target list.

Name	EPIC number	Spec type	$T_{\rm eff}$ (K)	Mass ($M_\odot$)	Radius ($R_\odot$)	Mag (V)	$\log R'_{\rm HK}$	*K2* # FOV	# of RV
HD 173427	214112021	G1V	6244	1.189	1.367	8.57	–4.33	7	7
HD 181544	213410372	G1V	6212	1.218	1.603	7.11	–4.61	7	6
HD 177033	213812240	K2/K3V	5090	0.740	0.709	10.07	–4.66	7	3
HD 6101	220417763	K2V	4991	0.844	0.781	8.131	–4.76	8	4
HD 6480	220409971	F5/7 V	5970	1.081	1.159	7.25	–4.86	8	12
HD 183877	213873758	G8V	5748	1.009	0.977	7.15	–4.94	7	7
HD 4628	220429217	K2.5V	5057	0.787	0.731	5.74	–4.94	8	5
HD 4256	220260370	K3V	5047	0.828	0.760	8.001	–5.08	8	4
HD 179205	214776835	G1/2V	5988	0.882	0.977	8.59	–4.55	7	5

Notes. The table is ranked based on the target $\log R'_{\rm HK}$ values (decreasing).

and provided a relation to predict RV jitter for a given star as a function of $v \sin i$, spectral type, and photometric variability. Later, Boisse et al. (2009) and Lanza et al. (2011) performed simultaneous photometric and RV observations of HD 189733 and demonstrated that simultaneous photometric time series can deliver a wealth of information about the configuration and distribution of active regions on the surface of a star, and thus would allow us to improve our understanding of the RV jitter. However, it is important to remember that HD 189733 is a very active star and, therefore, the conclusion of these studies could not easily be extrapolated to other stars with different activity levels, and in particular to relatively low-activity stars like our Sun.

To further study the relationship between photometric variability and the expected level of RV jitter, Cegla et al. (2014) used high-precision light curves from the *Kepler* space telescope. Unfortunately, due to the faintness of stars in the *Kepler* field, direct RV measurements were unavailable for most targets. To counter this, these authors used readily available GALEX UV flux measurements and a series of empirical relationships (between excess UV flux, the calcium activity indicator ($\log R'_{\rm HK}$), and RV jitter) to indirectly estimate the RV jitter.

Later, Bastien et al. (2014) went one step further and collected the California Planet Search archival RV measurements of stars that lay in the *Kepler* field of view. They used high-precision RV measurements obtained at the Keck and Lick observatories and high-precision photometric observations of twelve *Kepler* stars. They searched for a common periodicity between RV jitter and photometric variability of each individual star. The major drawback of their study was that their RV measurements were not taken simultaneously with Kepler's photometric observations. From solar and stellar observations, it is well known that the stellar magnetic activity evolves as a function of time, even over a single solar rotation (e.g., Baliunas et al. 1995), and therefore observations performed during different epochs can be completely independent of measurements and may not exhibit any meaningful or physical correlations.

A new opportunity was provided by *K2*, which is an extended mission of the original *Kepler* space telescope (Borucki et al. 2010) after the failure of *Kepler*'s two reaction wheels. *K2* aims to observe different fields, all in the ecliptic plane, each for the duration of approximately 80 days (Howell et al. 2014). *K2* Campaign 7 and 8 fields of view were observed between 4 October and 26 December 2015, and between 3 January and 23 March 2016, respectively. *K2* Campaigns 7 and 8 were both positioned in the southern hemisphere, which provided us the unique opportunity to carry out simultaneous high-precision RV measurements with the HARPS spectrograph mounted on the 3.6 m ESO telescope. We were allocated three nights of observation time with HARPS to execute RV measurements simultaneously with *K2* observations of nine stars.

The main goal of the current paper is to identify and characterize the possible correlation between photometric variability and RV jitter, using simultaneous space-based *K2* high-precision photometry and HARPS high-precision RV measurements. Such a full characterization and relationship will be crucial to selecting the best transiting candidates, to be followed up by RV observations, for upcoming missions such as TESS (Ricker et al. 2014) and PLATO 2.0 (Rauer et al. 2014), and will greatly improve the efficiency of the RV follow-up of planet candidates with the next generation of stabilized spectrographs such as ESPRESSO (Pepe et al. 2014). We also explore the variation of different activity indicators, such as direct chromospheric activity indicator ($\log R'_{\rm HK}$), and atmospheric line profile diagnostics such as BIS and FWHM.

We organize this paper as follows. In Sect. 2 we describe our observational datasets. In Sect. 3 we assess the correlation between the RV measurements, photometric variation, FWHM, BIS, $\log R'_{\rm HK}$, and 8-h flicker. In Sect. 4, we examine and evaluate two main modeling approaches, namely *FF′* (Aigrain et al. 2012) and *SOAP2.0* (Dumusque et al. 2014), for modeling activity-induced RV jitter. In Sect. 5 we present the analysis of a star that we observed in the spectropolarimetric mode of HARPS in order to estimate its magnetic field of star and test for correlations with the RVs. Finally, in Sect. 6 we summarize and draw conclusions on our results.

2. Observations and data reduction

2.1. Target selection

We created a list of potential targets by cross-matching the stars that had an activity level characterized through the $\log R'_{\rm HK}$ index based on archival HARPS spectra and the approved targets for Campaigns 7 and 8 of *K2*. From this list we tried to select stars with different activity levels, from very active ($\log R'_{\rm HK} > -4.6$) to quiet ones ($\log R'_{\rm HK} < -4.8$). Our final sample contains nine stars. In Table 1 we list the main stellar parameters of our targets; some of these parameters were obtained through the *K2* Ecliptic Plane Input Catalog (EPIC)[1].

2.2. K2 data

We downloaded the pixel data of all of our targets from the Mikulski Archive for Space Telescopes (MAST)[2], and then

[1] https://archive.stsci.edu/k2/epic/search.php
[2] https://archive.stsci.edu/k2/

utilized a modified version of the CoRoT imagette pipeline (known as POLAR) to extract the high-precision photometric time series. A full description of the POLAR pipeline is presented in Barros et al. (2016), and this pipeline has been used in several exoplanet discoveries from *K2* (e.g., Barros et al. 2015; Armstrong et al. 2015; Lillo-Box et al. 2016; Santerne et al. 2016; Bayliss et al. 2017). The stars analyzed in this study are very bright and were almost all saturated in the *K2* data; therefore, we adapted the apertures to include all the flux for the star[3]. Furthermore, we checked the co-detrending vectors to make sure that the variability in the light curves did not include instrumental effects.

2.3. HARPS observations

We were allocated three nights on the HARPS spectrograph, mounted on the ESO 3.6 m telescope at La Silla observatory (Mayor et al. 2003) to carry out high-precision RV measurements of all of our targets (under ESO program ID 096.C-0708(A), PI: M. Oshagh). Thanks to the time-sharing scheme on HARPS with several other observing programs, we managed to spread our observations over 50 nights from 5 October 2015 to 1 November 2015, and from 8 January 2016 to 3 February 2016.

The collected HARPS spectra were reduced using the HARPS Data Reduction Software (DRS; Pepe et al. 2002; Lovis & Pepe 2007). In the DRS the spectra were cross-correlated with masks based on the target's stellar spectral type. As output the DRS provides the RVs, FWHM of the cross-correlation function (CCF), BIS (as defined in Queloz et al. 2001), $\log R'_{\rm HK}$ (as described in Lovis et al. 2011), and their associated uncertainties following the methods described in Bouchy et al. (2001).

We decided to observe one of our stars (HD 179205) in the spectropolarimetric mode of HARPS (HARPS-Pol) instead of the standard RV mode. Spectropolarimetric observations enable us to estimate the stellar magnetic field. Therefore, we exclude this star from our analysis in Sects. 3 and 4; however, we dedicate a separate section (Sect. 5) for a detailed analysis of this star.

Figure 1 presents simultaneous high-precision *K2* photometric time series, RV, FWHM, BIS, and $\log R'_{\rm HK}$ for each of the eight stars in our sample. We note that the scale of photometric variability, which is shown in the top panels in all plots in Fig. 1, covers a diverse range of values depending on each star's photometric variability. Therefore, caution should be used when comparing the photometric variability of the stars to one another.

3. Probing the correlations between RVs and other observables

3.1. Flux, FWHM, BIS, and $\log R'_{\rm HK}$

In this section we assess the presence of any meaningful correlation between all the observables versus the high-precision HARPS RV measurements for each individual star. We inspect the presence of a correlation based on Spearman's rank-order correlation coefficient (ρ)[4]. Moreover, we evaluate the significance of the measured ρ using the straightforward Bayesian approach described in Figueira et al. (2016). The posterior distribution of ρ indicates the range of ρ values that is compatible with the observations. In particular, it allows us to assess how probable a non-zero correlation value is.

Figures 2 and B.1 present the correlations between the RV measurement of each star and the corresponding photometric variation, FWHM, BIS, and $\log R'_{\rm HK}$. In the top right corner of each panel, the posterior distribution of ρ and its most probable value are presented. The dashed vertical lines indicate the 68% highest posterior density credible intervals (Figueira et al. 2016).

As can be seen for the case of very active stars such as HD 173427, there are strong (as reported by the high absolute value of the average ρ) and quite significant (as reported by its lower spread, narrower credible intervals, and incompatibility of the average value with zero) correlations between the measured RVs and all the simultaneously obtained observables, except the photometeric variability. As we move towards lower activity levels (as indicated by lower photometric variability, lower RV jitter rms, or smaller values of $\log R'_{\rm HK}$), the correlations become random. For instance, our result shows very strong correlation between the RV and BIS for the very quiet star (HD 4256), and on the contrary shows no correlation between RV and BIS for the second most active star in our sample (HD 181544). Therefore, from our results it is hard to conclude any trend or behavior for the correlation between RV and other observables depending on the stellar activity level. In the quest for exoplanets, especially in RV surveys, quiet stars (as determined by low levels of photometric variability or low level of activity determined based on their $\log R'_{\rm HK}$) are traditionally favored and targeted. However, our result suggests that the challenge might also be disentangling the quiet stars' activity-induced RV from the planetary RV signal, due to the lack of strong correlations between the RV jitter and any other observables. We list all the correlation coefficients and their 68% highest posterior density credible intervals in Table 2.

However, if we choose to determine the best activity indicator by exclusively inspecting carefully all the correlations presented in Table 2 and Fig. 2, we can state that the FWHM appears to be the best indicator. This is backed by the common idea that the correlation between FWHM and RVs (even though not very strong or significant consistently) persists for stars of different activity levels. Our conclusion about the FWHM is in strong agreement with the findings of Queloz et al. (2009) and Pont et al. (2011), who also suggested that the FWHM should be used to reconstruct the RV jitter.

We would like to note that a phase shift is expected between the RV measurements and some of the other observables, due to geometrical or physical processes. For instance, Queloz et al. (2001) and Santos et al. (2003) were the first to pinpoint the presence of a phase shift between photometry and RV signal. In addition, Queloz et al. (2009) estimated a phase shift of one-quarter of the stellar rotation between FWHM and RV measurements of CoRoT-7. The presence of a phase shift might affect the correlation between two observables and we evaluate this in Appendix A. However, the low number of spectroscopic observations for each individual star in our sample prevents us from exploring any type of periodicity test on them as well as assessing the existence of phase shift in them and also investigating its impact on our analysis. Moreover, it is worth mentioning that the inclination angle of the stellar rotation axis might also influence the presence and strength of the correlations between RVs and other observables; however, since the stellar inclination values

[3] We extend the aperture at the bottom and the top of saturated columns to ensure that no photo-electron smearing from the saturated pixels is lost throughout the campaign.

[4] Spearman's rank-order correlation assesses how well two variables can be described with a monotonic relationship and not a purely linear one.

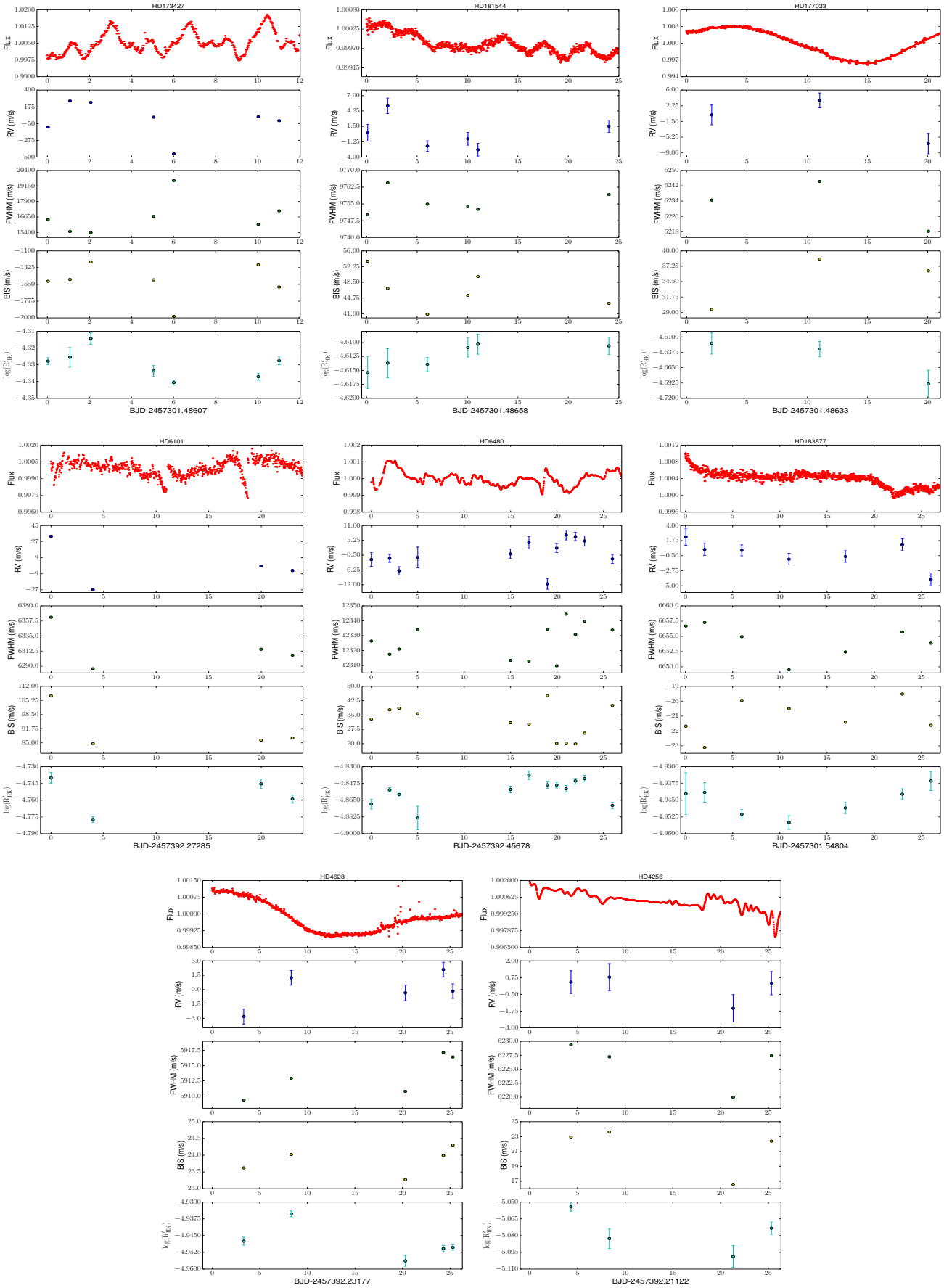

Fig. 1. Simultaneous high-precision *K2* photometric time series, RV, FWHM, BIS, and $\log R'_{\rm HK}$ for each star in our sample. Sorted by increasing activity level based on $\log R'_{\rm HK}$. We note the different scales of photometric variability in each of the top panels. In some cases the error bars are smaller then the symbol size.

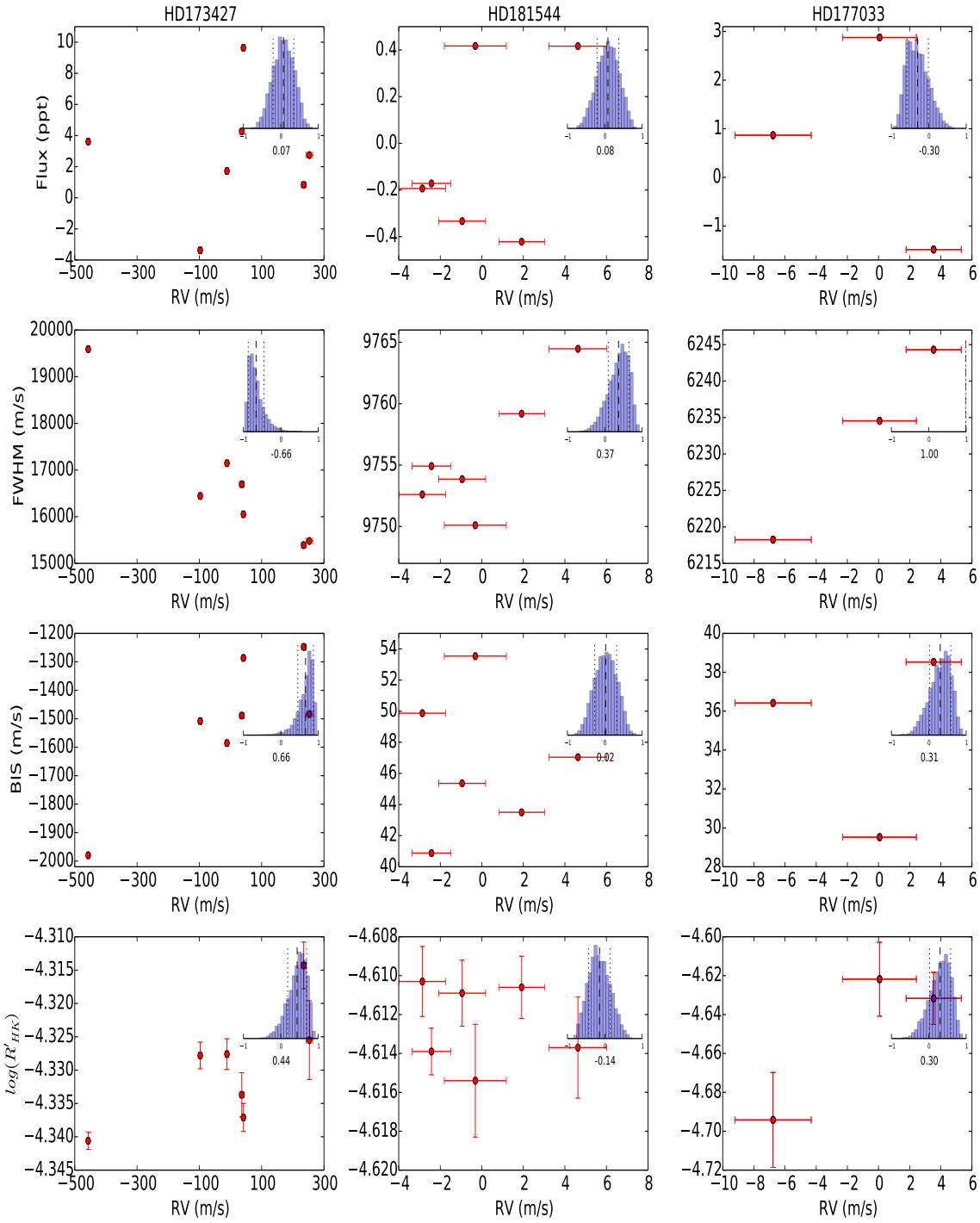

Fig. 2. Correlations between the RV measurements and the corresponding photometric variations FWHM, BIS, and $\log R'_{\rm HK}$. They are sorted by increasing activity level based on $\log R'_{\rm HK}$. At the top right of each panel the calculated value of ρ and also its posterior distribution is presented. The dashed vertical lines indicate the 68% highest posterior density credible intervals (Figueira et al. 2016). The total sample is shown in Fig. B.1.

of our targets are not known, exploring this possibility is beyond the scope of this paper.

3.2. F8

The term "8-h flicker" or simply "F8", which is defined as the RMS of photometric observations on time scales shorter than 8 h, was introduced by Bastien et al. (2013). Bastien et al. (2013) found that the F8 values exhibit a strong correlation with the surface gravity of the stars determined asteroseismically, and thus proposed the idea of using the F8 value to estimate the stellar surface gravity. Moroever, Bastien et al. (2014) also identified a tentative correlation between the F8-based stellar surface gravity and the RV jitter. Furthermore, Cegla et al. (2014) explored the possible correlation between the F8 and RV jitter and also between the F8 diagnostic and photometric variability, and also provided evidence that a temperature sensitive correlation exists for quiet stars. In this section we aim to assess possible correlations between the measured F8s and the RV jitter

Table 2. Calculated Spearman's rank-order correlation coefficients and their 68% highest posterior density credible intervals, sorted by increasing activity level based on $\log R'_{\rm HK}$.

Name	RV vs. FLUX	RV vs. *FWHM*	RV vs. BIS	RV vs. $\log R'_{\rm HK}$	$\log R'_{\rm HK}$
HD 173427	**0.07** ± 0.28	**–0.66** ± 0.20	**0.66** ± 0.20	**0.44** ± 0.31	–4.33
HD 181544	**0.08** ± 0.30	**0.37** ± 0.27	**0.02** ± 0.30	**–0.14** ± 0.27	–4.61
HD 177033	**–0.30** ± 0.29	**1.00** ± 0.0001	**0.31** ± 0.28	**0.30** ± 0.28	–4.66
HD 6101	**0.48** ± 0.30	**1.00** ± 0.0001	**0.47** ± 0.29	**1.00** ± 0.0001	–4.76
HD 6480	**0.16** ± 0.23	**0.07** ± 0.21	**–0.80** ± 0.10	**0.40** ± 0.21	–4.86
HD 183877	**0.21** ± 0.28	**0.57** ± 0.23	**–0.04** ± 0.28	**0.07** ± 0.25	–4.94
HD 4628	**–0.28** ± 0.29	**0.64** ± 0.24	**0.28** ± 0.30	**0.00** ± 0.29	–4.94
HD 4256	**0.32** ± 0.31	**0.21** ± 0.30	**1.00** ± 0.0001	**0.20** ± 0.25	–5.08

amplitude and also between F8 and the photometric variation amplitude.

We calculate the F8 value for all our targets according to the description provided by Bastien et al. (2013). As we mentioned in the introduction Bastien et al. (2014) performed a similar study using high-precision RV measurements obtained from Keck and Lick observatories, and high-precision photometric observations of 12 *Kepler* stars. Although their RV measurements were not taken simultaneously with *Kepler*'s photometric observations, their stars do cover a wide range of stellar activity (though most are in the low-activity regime)[5]. Therefore, here we decided to combine their stars with our sample and study them together[6].

Figure 3 presents the correlation between the measured F8 and their corresponding RV jitter and photometric variation amplitudes. We examined the correlation between the variables, as was done in Sect. 3 and Fig. 2, by evaluating the posterior distribution of Spearman's correlation coefficient ρ; its most probable values are presented. As Fig. 3 shows, the F8 values of stars in our sample exhibit strong and significant correlations with the RV jitter and photometric variation amplitude (shown as the filled circles, green histograms, and green values in Fig. 3). When we combine our targets with Bastien et al. (2014) and evaluate the total sample the correlation between F8 and RV jitter becomes stronger and more significance, and on the other hand the correlation between F8 and photometric variation becomes much weaker and also less significant. Therefore, our results indicate that F8 might be a powerful proxy for activity-induced RV over a wide range of stellar activity. However, we would like to note that the Bastien et al. (2014) stars were mostly from the low-activity regime (based on their low photometric variability and also RV jitter amplitude) and a lack or presence of correlation in the low-activity regime may have diluted or strengthened the total correlation. Moreover, the Bastien et al. (2014) RV measurements were not taken simultaneously with *Kepler*'s photometric observations; this delay would lead to an artificial correlation in the Bastien et al. (2013) sample, and thus could bias the total correlation.

We also attempted to evaluate the dependence of correlations on the stellar temperatures, as presented by the color-coded points in Fig. 3. However, we could not identify any meaningful trend between the correlations and stellar temperatures.

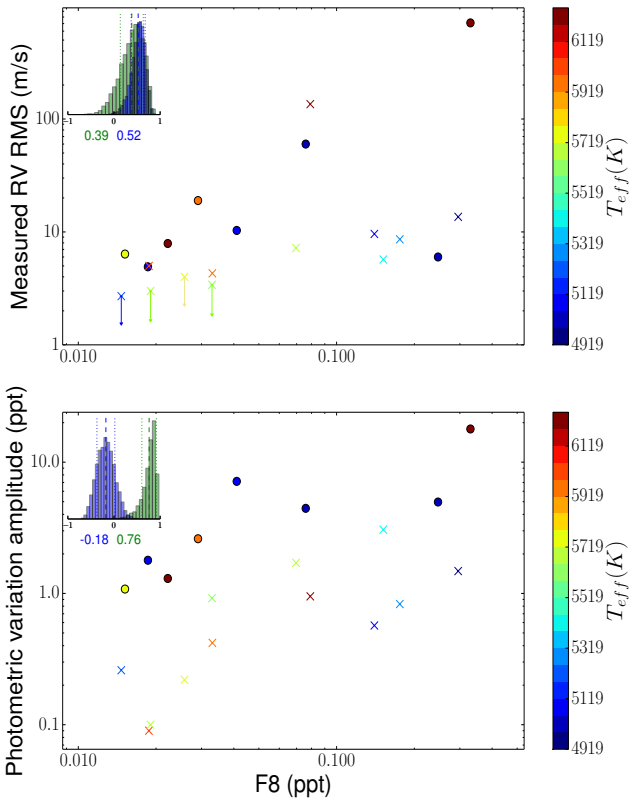

Fig. 3. *Top*: correlation between measured F8 values and RV jitter amplitude of our targets (filled circles) and the stars from Bastien et al. (2014; crosses). At the top left are presented the calculated value of ρ and also its posterior distribution for our targets (green histogram and green value) and for the full sample (blue histogram and blue value). The RV jitter values reported in Bastien et al. (2014) with values less than 4 m s^{-1} are considered as the upper limits, and are indicated by descending arrows in this plot. The points are color-coded according to their $T_{\rm eff}$. *Bottom*: same as the top, but for the F8 and photometric variation amplitude.

4. Modeling

In this section we assess how accurately the RV jitter amplitude can be predicted using the simultaneous high-precision photometric time series and by applying two different modeling techniques, namely *FF′* and *SOAP2.0*, across different levels of stellar activity.

[5] As mentioned in Bastien et al. (2014), the RV jitter presented with values lower than 4 m s^{-1} may be dominated by instrumental systematics and shot noise. Therefore, these values are considered as upper limits.

[6] We used the F8 values for the Bastien et al. (2014) stars which were obtained via private communication because the values published in Bastien et al. (2016) catalog for these stars are incorrect (Bastien, priv. comm.). An erratum of the Bastien et al. (2016) catalog is in preparation.

4.1. The FF′ method

The FF' method, which was introduced by Aigrain et al. (2012), provides a simple technique to predict the RV jitter from simultaneous photometric time series and its first derivative. This method considers two main components: a rotational one, and another arising from convective blueshift variations. The rotational term estimates the RV due to the contrast of active regions on the rotating star, and can be shown to be given by, as in Aigrain et al. (2012),

$$\Delta RV_{\rm rot}(t) = -\frac{\dot{\psi}(t)}{\psi_0}\left[1-\frac{\psi(t)}{\psi_0}\right]\frac{R_\star}{f}, \quad (1)$$

where $\psi(t)$ is the flux and $\dot{\psi}(t)$ its first derivative, $R_\star$ is the stellar radius in solar radii, ψ_0 is the maximum of $\psi(t)$ when there are no spots on the visible part of the star, and f is the reduction in the flux which is equal to the fractional area of a spot to the stellar disk.

The convective blueshift term takes into account the impact of suppression of convective blueshift in the active region's area. Following Aigrain et al. (2012), this can be formulated as

$$\Delta RV_{\rm CB}(t) = \left[1-\frac{\psi(t)}{\psi_0}\right]^2\frac{\delta V_{\rm c}\kappa}{f}, \quad (2)$$

where $\delta V_{\rm c}$ is the difference of the convective blueshift velocity between inactive and active regions and κ is the ratio of the unspotted area to the active region area (typically $\gg$1).

Therefore, the total activity-induced RV prediction of the FF' method can be estimated as

$$\Delta RV_{\rm activity}(t) = \Delta RV_{\rm rot}(t) + \Delta RV_{\rm CB}(t). \quad (3)$$

We compared the amplitude of the FF' predicted RV jitter to the amplitude of the observed RV jitter for each individual star in our list of targets. To do this we first smoothed the photometric observations (using an iterative nonlinear filter; Aigrain & Irwin 2004) and calculated its first derivative for each star. We adopted the stellar radius reported in Table 1 for Eq. (1). Since the exact values of f, $\delta V_{\rm c}$, and κ are not known, they are treated as free parameters. We obtain their value by fitting the maximum and minimum of the FF' predicted RVs to the maximum and minimum of the observed RVs, respectively, using an Levenberg-Marquardt algorithm. We would like to note that these parameters have some boundaries due to their definitions and physical constraints. For instance, f has to be in the range of [0, 1]; therefore, we set those boundaries to prevent the fitting procedure from attempting to obtain non-physical values.

4.2. The SOAP tool

SOAP is a publicly available tool that simulates the effects of dark spots and bright plages on the surface of a rotating star by taking into account the flux contrast effect (Boisse et al. 2012). *SOAP 2.0* is an upgraded version of *SOAP*[7]. *SOAP 2.0* can generate the photometric and RV variation signals induced by active regions by taking into account the flux contrast effect in those regions, and also the RV shift due to inhibition of the convective blueshift inside those regions (Dumusque et al. 2014). Dumusque et al. (2014) demonstrated that the RV jitter of a spot-dominated star is dominated by the temperature contrast of spots combined with the stellar rotation; however, for the case of a plage-dominated star the inhibition of convective blueshift takes over. Therefore, we can consider the *SOAP2.0* tool to be the numerical equivalent of the FF' approach, which attempts to simulate the two main effects (flux contrast and suppression of convective blueshift).

SOAP 2.0 allows us to predict the amplitude of RV jitter from the photometric time series. To do so, first we adjusted all the required stellar parameters in *SOAP2.0* according to their value from Table 1. We assumed a single spot[8] on the stellar surface with a fixed temperature contrast of −663 K, corresponding to the average temperature contrast between a sunspot and a quiet region on the Sun as determined by Meunier et al. (2010). Then we varied the spot's size until the photometric output of *SOAP2.0* matched the amplitude variation of the observed light curve. At that point we compared the predicted RV jitter from *SOAP2.0* to the observed value. We repeated the same procedure assuming a single plage with a temperature contrast of +250 K on the stellar surface instead of a spot. Meunier et al. (2010) showed that the temperature contrast of a plage located at the solar disk center was +250 K. We would like to note that due to the smaller temperature contrast of plages compared to those of spots, the required plage filling factor needed to generate the same photometric variability as spots is usually much larger, often by a factor of four, than the spot-filling factor. This photometric constraint has clear implications: due to larger areas in which the inhibition of convective blueshift occurs, a plage results in a much larger RV jitter amplitude compared to a single spot.

4.3. Comparison of predicted and observed RV jitter

In this section we assess the ability of the FF' and *SOAP2.0* methods in predicting the amplitude of RV jitter from simultaneous photometry time series. Figure 4 presents the amplitude of predicted over observed RV jitter as a function of photometric variability (shown by the markers with circles).

As we mentioned earlier, Bastien et al. (2014) performed a similar study using high-precision RV measurements obtained from Keck and Lick observatories, and high-precision photometric observations of 12 stars observed by *Kepler*. Even though their RV measurements were not taken simultaneously with *Kepler*'s photometric observations, their choice of stars covered a wider activity value range towards the lower activity regime. Therefore, we decided to repeat the procedures presented in Sects. 4.1 and 4.2 on their observations and to overplot the result for their targets in Fig. 4 (shown by the markers without surrounding circles).

As Fig. 4 presents, it is clear that the FF' method systematically underpredicts the RV jitter amplitude for the whole range of photometric variabilities considered, and particularly for the low-activity stars (as measured by their photometric variability). This finding is in strong agreement with the Bastien et al. (2014) result. The accuracy of the *SOAP2.0* models strongly depend on the level of photometric variability. For instance, *SOAP2.0* predicions arising from the single-spot model improves significantly when the photometric variability is above a 1 ppt limit. On the contrary for quiet stars, when the photometric variability

[7] The tool is publicly accessible through `www.astro.up.pt/resources/soap2/`

[8] Since we are interested in modeling the total amplitude of photometric variability and RV jitter, the inclusion of multiple spots/plages with total filling factor as a single spot/plage (to generate the observed amplitude) just broadens the shape of the photometric and RV signal and does not affect the amplitude of those signals, and thus does not provide extra information.

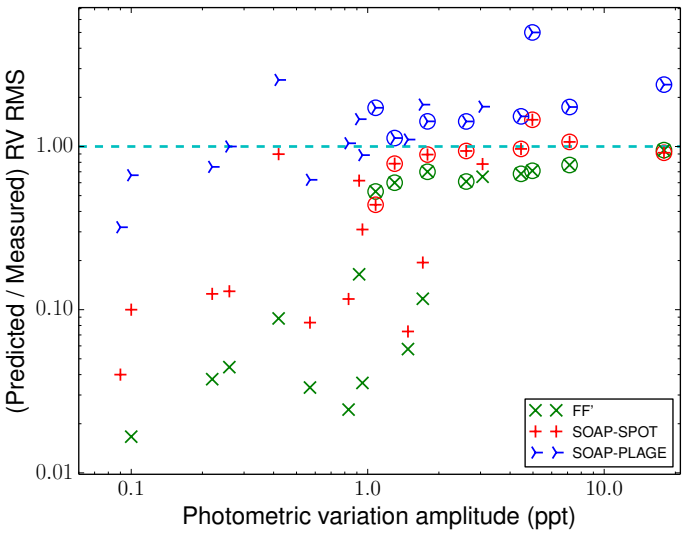

Fig. 4. Predicted vs. observed RV rms as a function of photometric variability. The green ×'s denote the *FF′* method predictions, red pluses show *SOAP2.0* single-spot model, and blue triangles (right) displays the *SOAP2.0* single-plage model. The stars from our sample are presented by the markers enclosed in circles and the results from analyzing stars from Bastien et al. (2014) are presented by the markers without surrounding circles.

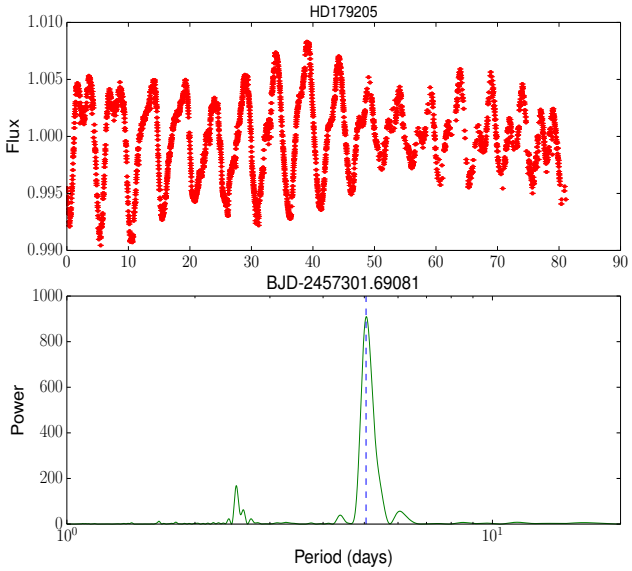

Fig. 5. *Top*: entire *K2* photometric time series of HD 179205 spanning almost 80 days. *Bottom*: GLS periodogram of the photometric time series. The dashed line indicates the exact value of the peak of the periodogram corresponding to the stellar rotation period.

is smaller than 1 ppt, the *SOAP2.0* single-plage model provides more accurate predictions, while overestimating the RV jitter for photometrically active stars. Thus, our results can be interpreted as the confirmation of the presence of two distinctly different activity regimes, spot-dominated and plage-dominated, and are in strong agreement with studies such as Lockwood et al. (1997), Radick et al. (1998), and Shapiro et al. (2016), which suggested a transition between spot-dominated activity for stars at higher activity levels and plage-dominated activity at lower activity levels.

5. Spectropolarimetric observation of HD 179205

As mentioned earlier, one of our targets (HD 179205) was observed in the spectropolarimetric mode of HARPS (HARPS-Pol) instead of standard RV measurements in order to enable us to measure the line-of-sight-projected magnetic field averaged over the visible hemisphere of the star (also called longitudinal field or B_l). Although B_l is no more than a first-order magnetic proxy unable to capture the full complexity of the field topology, it can still be used to get a first hint of the large-scale field at the surface of the star when Stokes *V* signatures are reliably detected at the surface of the star.

We first tried to estimate accurately the stellar rotation period of HD 179205. To this end we utilized the entire *K2* photometric time series of HD 179205 and then applied the Generalised Lomb-Scargle periodogram (Zechmeister & Kürster 2009). Figure 5 presents the whole *K2* light curve and also the resulting periodogram, which exhibits a significant peak at 5.047 days. Thus, we estimated $P_{\rm rot} = 5.047 \pm 0.15$ days (the error was estimated from the full width at half maximum of the peak in the periodogram), which indicates that HD 179205 is a moderately rapidly rotating star. In order to ensure that our estimated value for the stellar rotation is accurate and it is not its first harmonic $P_{\rm rot}/2$, we used the relation provided by Noyes et al. (1984) to estimate the stellar rotation based on the stellar $B - V$ and $\log R'_{\rm HK}$. Assuming $B - V = 0.55$ and $\log R'_{\rm HK} = -4.55$, we estimated $P_{\rm rot} = \sim 5.9$ days, which is in broad agreement with our estimate.

In the spectropolarimetric mode, each spectropolarimetric observation consists of a sequence of four subexposures recorded with the polarimeter quarter-wave plate set to different pre-selected azimuths. By applying least-squares deconvolution (LSD; Donati et al. 1997) to the observed spectra, we obtained Stokes *I* and *V* LSD profiles, allowing us to estimate the B_l at each observing epoch. Despite reaching error bars as low as a few G on B_l, the field of HD 179205 is not reliably detected in any of our observing epochs. This is not surprising given the spectral type and rotation period of the star, for which typical B_l values of no more than a few G are to be expected, thus requiring sub-G error bars on B_l for a definite detection.

Figure 6 shows the simultaneous *K2* high-precision photometric and longitudinal magnetic field estimation and RV variations. Our results demonstrate how difficult it is to detect and estimate B_l with enough precision for RV filtering studies.

Future studies with near-IR spectropolarimeters like SPIRou at CFHT should be able to reach improved precisions on B_l (thanks to the larger Zeeman splitting at infrared wavelengths), and also to detect the Zeeman broadening of spectral lines giving access to the unsigned magnetic flux at the surface of the star, thought to be one of the best proxies for the RV activity jitter (Haywood et al. 2016).

6. Conclusion

In this paper we present simultaneous high-precision photometric observations (taken with the *K2* space telescope) and RV measurements (obtained with the HARPS spectrograph) for a sample of nine stars. We first assessed the presence of any meaningful relationships between the measured RV jitter and the simultaneous photometric variations, and between other activity indicators (such as BIS, FWHM, and $\log R'_{\rm HK}$), by evaluating the

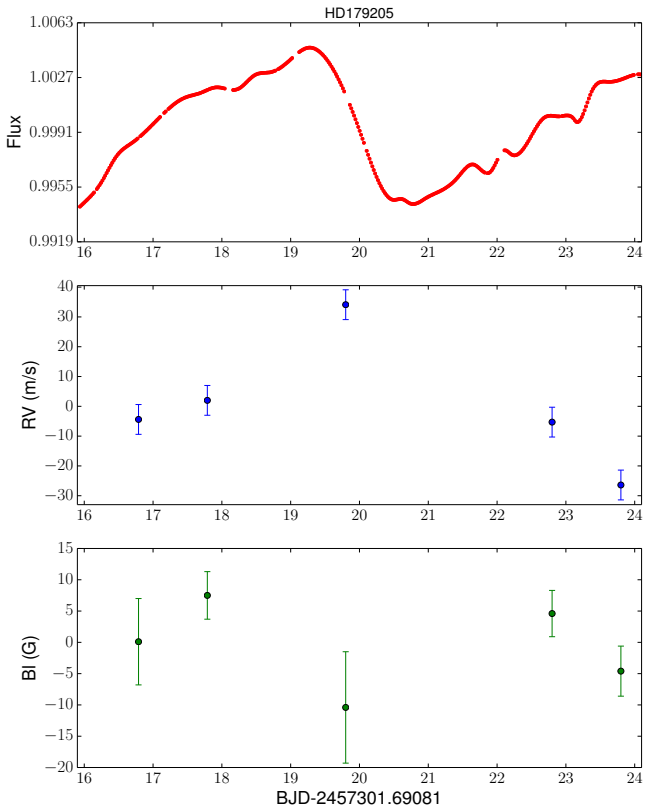

Fig. 6. Simultaneous high-precision *K2* photometric time series, RV, and B_l of HD 179205.

strength and significance of the correlation between each of the observables.

We found that strong and significant correlations exist between almost all the observables and the measured RVs for the very active star in our sample and, therefore, they can (in principle) all be used as a proxy for activity. However, as we move towards lower stellar activity levels the correlations become random, and we could not reach a conclusion regarding the tendency of correlations depending on the stellar activity level. Traditionally, quiet stars are favored targets for exoplanet searches; however, our result suggests that it can be challenging to disentangle their activity-induced RVs from the planetary RV signal. We further calculated the F8 values of all our targets, and illustrated that F8 exhibits a distinct and strong correlation with the RV jitter, and not strong correlation with the photometric variability amplitude. Therefore, our results indicated that F8 could be used as a good proxy for estimating the amplitude of RV jitter. This finding is in agreement with the previous work of Bastien et al. (2014) and Cegla et al. (2014).

Moreover, we examined the capability of two state-of-the-art modeling techniques, namely the *FF′* method and *SOAP2.0*, to accurately predict the RV jitter amplitude using simultaneous photometric observations. We conclude that for very active stars both techniques can predict the amplitude of RV jitter reasonably well. Furthemore, we find that the *FF′* method systematically underpredicts the RV jitter amplitude across the whole range of photometric variability levels considered, and this is particularly apparent for the low-activity stars in our sample. This finding is in strong agreement with the Bastien et al. (2014) result. Furthermore, the accuracy of the *SOAP2.0* predictions assuming a single-spot model improves significantly when the photometric variability rises above the 1 ppt limit. On the contrary for quiet stars, when the photometric variability is smaller than 1 ppt, the *SOAP2.0* single-plage model provides more accurate predictions. Thus, our results provide stronger evidence of (and support of) the existence of an activity level boundary where spots are spot-dominated at higher activity levels, transitioning to plage-dominated at lower activity levels.

Acknowledgements. M.O. acknowledges research funding from the Deutsche Forschungsgemeinschft (DFG, German Research Foundation) – OS 508/1-1. This work was supported by Fundação para a Ciência e a Tecnologia (FCT, Portugal) through the research grant for national funds and by FEDER through COMPETE2020 by grants UID/FIS/04434/2013 & POCI-01-0145-FEDER-007672, PTDC/FIS-AST/1526/2014 & POCI-01-0145-FEDER-016886 and PTDC/FIS-AST/7073/2014 & POCI-01-0145-FEDER-016880. P.F., N.C.S., V.A., and S.B. acknowledge support from FCT through Investigador FCT contracts Nos. IF/01037/2013CP1191/CT0001, IF/00169/2012/CP0150/CT0002, IF/00650/2015/CP1273/CT0001, and IF/01312/2014/CP1215/CT0004. P.F. also acknowledges support from Fundação para a Ciência e a Tecnologia (FCT) in the form of an exploratory project of reference IF/01037/2013CP1191/CT0001. P.F. acknowledges support from FCT transnational cooperation program Pessoa. M.O. also acknowledges the support of COST Action TD1308 through STSM grant with reference Number:STSM-TD1308-030416-077992. H.M.C. acknowledges the financial support of the National Centre for Competence in Research "PlanetS" supported by the Swiss National Science Foundation (SNSF). C.A.W. acknowledges support from the STFC grant ST/P000312/1. We would like to thank the anonymous referee for the insightful suggestions, which added significantly to the clarity of this paper. Last but not least, we would like to thank Fabienne A. Bastien for kindly providing the F8 measurements of stars in Bastien et al. (2014).

References

Aigrain, S., & Irwin, M. 2004, MNRAS, 350, 331
Aigrain, S., Pont, F., & Zucker, S. 2012, MNRAS, 419, 3147
Armstrong, D. J., Santerne, A., Veras, D., et al. 2015, A&A, 582, A33
Baliunas, S. L., Donahue, R. A., Soon, W. H., et al. 1995, ApJ, 438, 269
Barros, S. C. C., Almenara, J. M., Deleuil, M., et al. 2014, A&A, 569, A74
Barros, S. C. C., Almenara, J. M., Demangeon, O., et al. 2015, MNRAS, 454, 4267
Barros, S. C. C., Demangeon, O., & Deleuil, M. 2016, A&A, 594, A100
Bastien, F. A., Stassun, K. G., Basri, G., & Pepper, J. 2013, Nature, 500, 427
Bastien, F. A., Stassun, K. G., Pepper, J., et al. 2014, AJ, 147, 29
Bastien, F. A., Stassun, K. G., Basri, G., & Pepper, J. 2016, VizieR Online Data Catalog, 181
Bayliss, D., Hojjatpanah, S., Santerne, A., et al. 2017, AJ, 153, 15
Boisse, I., Moutou, C., Vidal-Madjar, A., et al. 2009, A&A, 495, 959
Boisse, I., Bouchy, F., Hébrard, G., et al. 2011, A&A, 528, A4
Boisse, I., Bonfils, X., & Santos, N. C. 2012, A&A, 545, A109
Borucki, W. J., Koch, D., Basri, G., et al. 2010, Science, 327, 977
Bouchy, F., Pepe, F., & Queloz, D. 2001, A&A, 374, 733
Cegla, H. M., Stassun, K. G., Watson, C. A., Bastien, F. A., & Pepper, J. 2014, ApJ, 780, 104
Czesla, S., Huber, K. F., Wolter, U., Schröter, S., & Schmitt, J. H. M. M. 2009, A&A, 505, 1277
Díaz, R. F., Ségransan, D., Udry, S., et al. 2016, A&A, 585, A134
Donati, J.-F., Semel, M., Carter, B. D., Rees, D. E., & Collier Cameron, A. 1997, MNRAS, 291, 658
Dumusque, X., Lovis, C., Ségransan, D., et al. 2011, A&A, 535, A55
Dumusque, X., Boisse, I., & Santos, N. C. 2014, ApJ, 796, 132
Figueira, P., Marmier, M., Bonfils, X., et al. 2010, A&A, 513, L8
Figueira, P., Faria, J. P., Adibekyan, V. Z., Oshagh, M., & Santos, N. C. 2016, Origins of Life and Evolution of the Biosphere, 46, 385
Haywood, R. D., Collier Cameron, A., Unruh, Y. C., et al. 2016, MNRAS, 457, 3637
Howell, S. B., Sobeck, C., Haas, M., et al. 2014, PASP, 126, 398
Huélamo, N., Figueira, P., Bonfils, X., et al. 2008, A&A, 489, L9
Lanza, A. F., Boisse, I., Bouchy, F., Bonomo, A. S., & Moutou, C. 2011, A&A, 533, A44
Lillo-Box, J., Demangeon, O., Santerne, A., et al. 2016, A&A, 594, A50
Lockwood, G. W., Skiff, B. A., & Radick, R. R. 1997, ApJ, 485, 789
Lovis, C., & Pepe, F. 2007, A&A, 468, 1115
Lovis, C., Dumusque, X., Santos, N. C., et al. 2011, ArXiv e-prints [arXiv:1107.5325]

Mayor, M., Pepe, F., Queloz, D., et al. 2003, The Messenger, 114, 20
Meunier, N., Desort, M., & Lagrange, A.-M. 2010, A&A, 512, A39
Noyes, R. W., Hartmann, L. W., Baliunas, S. L., Duncan, D. K., & Vaughan, A. H. 1984, ApJ, 279, 763
Oshagh, M., Santos, N. C., Boisse, I., et al. 2013, A&A, 556, A19
Oshagh, M., Santos, N. C., Ehrenreich, D., et al. 2014, A&A, 568, A99
Oshagh, M., Santos, N. C., Figueira, P., et al. 2015, A&A, 583, L1
Pepe, F., Mayor, M., Galland, F., et al. 2002, A&A, 388, 632
Pepe, F., Molaro, P., Cristiani, S., et al. 2014, Astron. Nachr., 335, 8
Pont, F., Aigrain, S., & Zucker, S. 2011, MNRAS, 411, 1953
Queloz, D., Henry, G. W., Sivan, J. P., et al. 2001, A&A, 379, 279
Queloz, D., Bouchy, F., Moutou, C., et al. 2009, A&A, 506, 303
Radick, R. R., Lockwood, G. W., Skiff, B. A., & Baliunas, S. L. 1998, ApJS, 118, 239
Rauer, H., Catala, C., Aerts, C., et al. 2014, Exp. Astron., 38, 249
Ricker, G. R., Winn, J. N., Vanderspek, R., et al. 2014, in Space Telescopes and Instrumentation 2014: Optical, Infrared, and Millimeter Wave, Proc. SPIE, 9143, 914320
Robertson, P., Mahadevan, S., Endl, M., & Roy, A. 2014, Science, 345, 440
Saar, S. H., Butler, R. P., & Marcy, G. W. 1998, ApJ, 498, L153
Santerne, A., Hébrard, G., Lillo-Box, J., et al. 2016, ApJ, 825, 55
Santos, N. C., Mayor, M., Naef, D., et al. 2002, A&A, 392, 215
Santos, N. C., Udry, S., Mayor, M., et al. 2003, A&A, 406, 373
Santos, N. C., Gomes da Silva, J., Lovis, C., & Melo, C. 2010, A&A, 511, A54
Santos, N. C., Mortier, A., Faria, J. P., et al. 2014, A&A, 566, A35
Shapiro, A. I., Solanki, S. K., Krivova, N. A., Yeo, K. L., & Schmutz, W. K. 2016, A&A, 589, A46
Zechmeister, M., & Kürster, M. 2009, A&A, 496, 577

Appendix A: Correlation and phase shift

In this appendix we probe the dependency of the correlation between two observables on the phase shift between them. To assess this we generated two identical sinusoidal signals and examined the variation of Spearman's rank-order correlation coefficient by introducing a phase shift between the two signals. Figure A.1 demonstrates how Spearman's correlation coefficient varies as a function of phase shift, and goes from a perfect correlation to anti-correlation in half a phase shift. Queloz et al. (2009) estimated a one-quarter stellar rotation phase shift between RVs and FWHM; therefore, in Fig. A.1 we present that region with a green shaded area. As can be seen, even a quarter of a stellar rotation phase difference between observables and RVs is sufficient to extinguish the strong correlation that might exist between them. However, we would like to note that activity signals are not typically sinusoidal, and therefore – even if they are not shifted – the correlation between RV and any indicator is usually not correlated with a 1:1 relation and the correlation coefficient will never be 1.

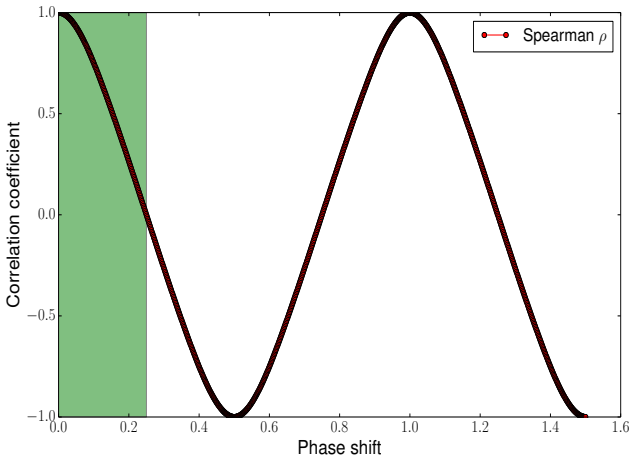

Fig. A.1. Variation of Spearman's correlation coefficient as a function of the phase shift between two identical sinusoidal signals. The green shaded area represents the one-quarter phase shift.

Appendix B: Correlations between the RV measurements and the corresponding photometric variations FWHM, BIS, and $log\ R'_{HK}$ for the whole sample

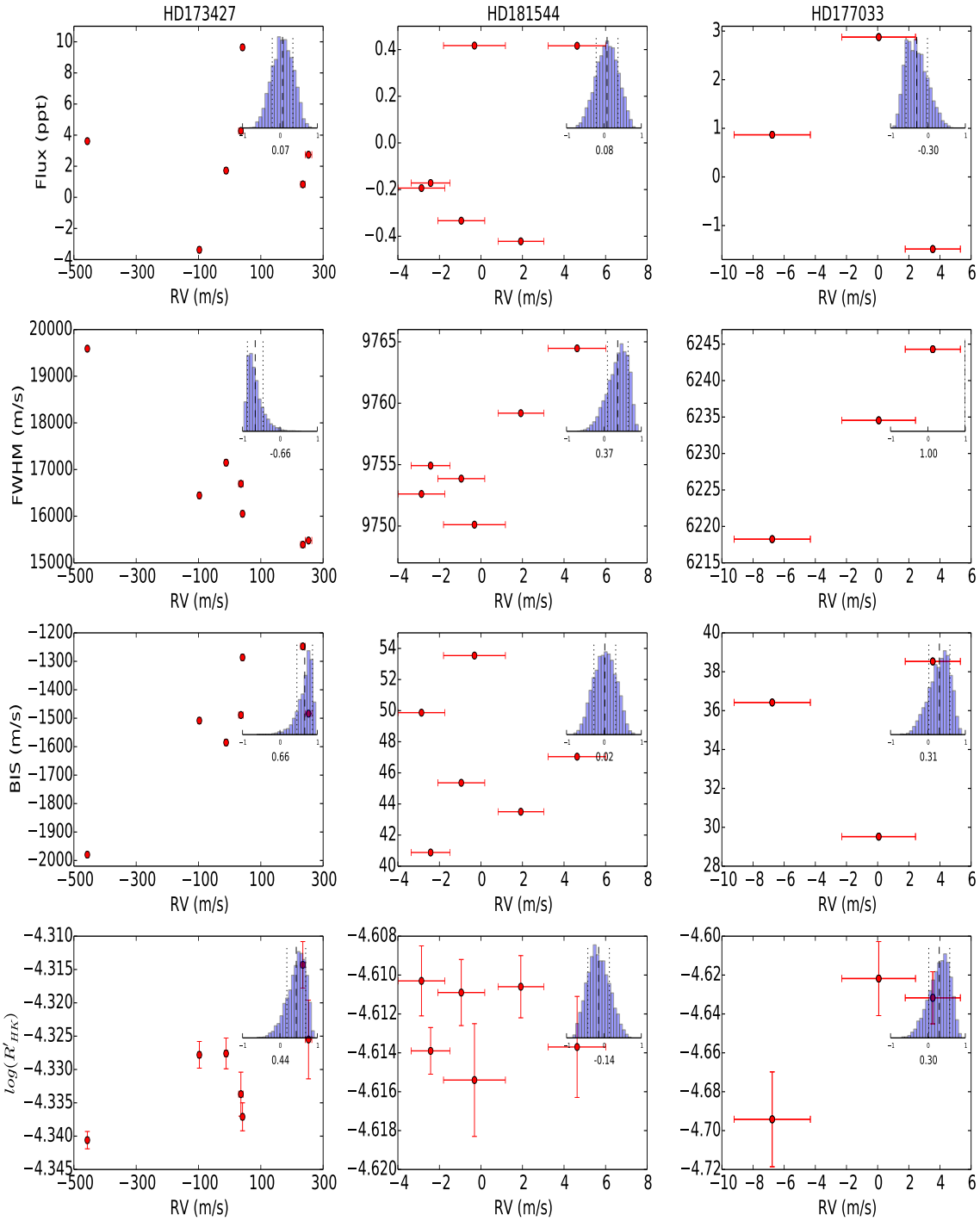

Fig. B.1. Same as Fig. 2 but for the whole sample.

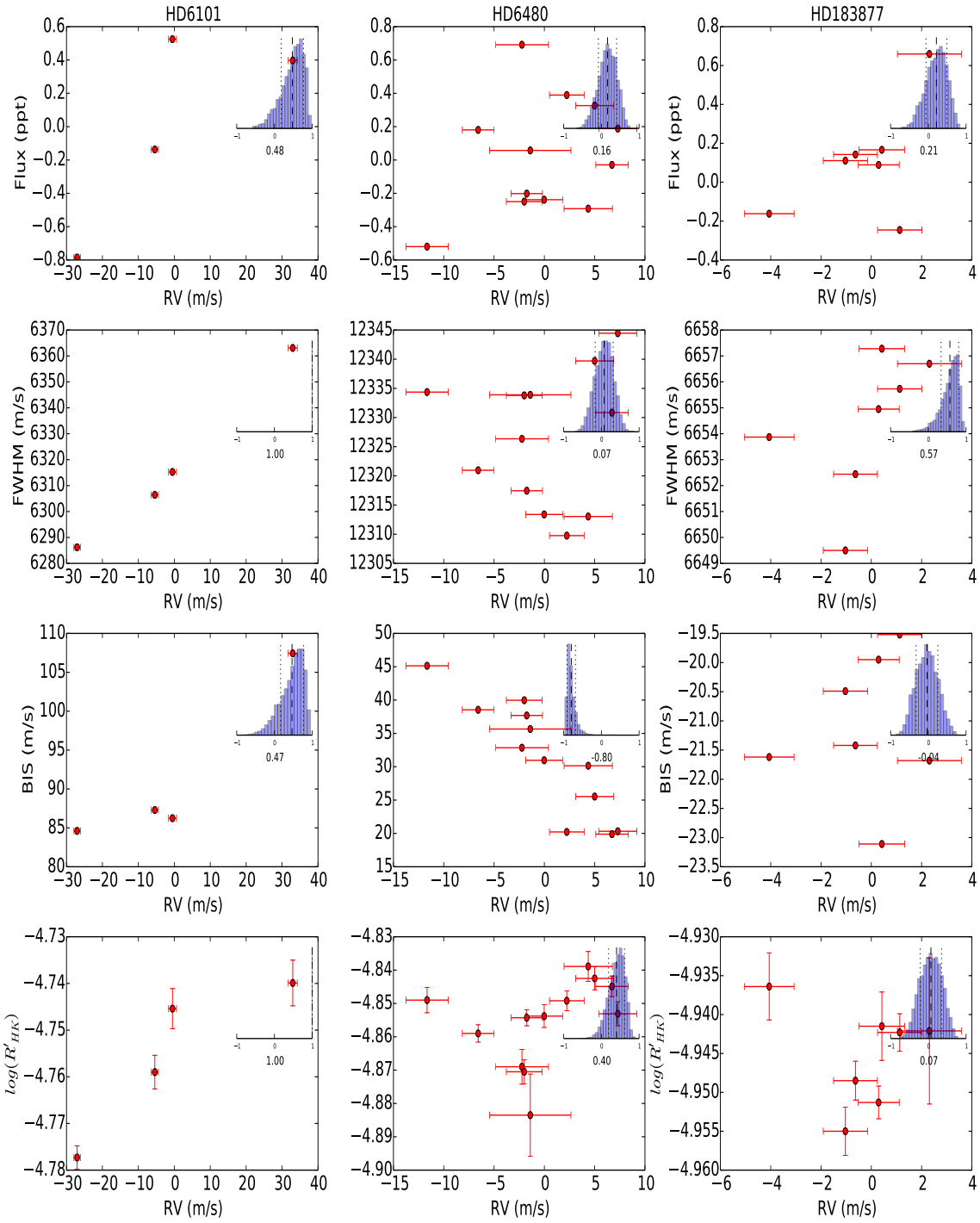

Fig. B.1. continued.

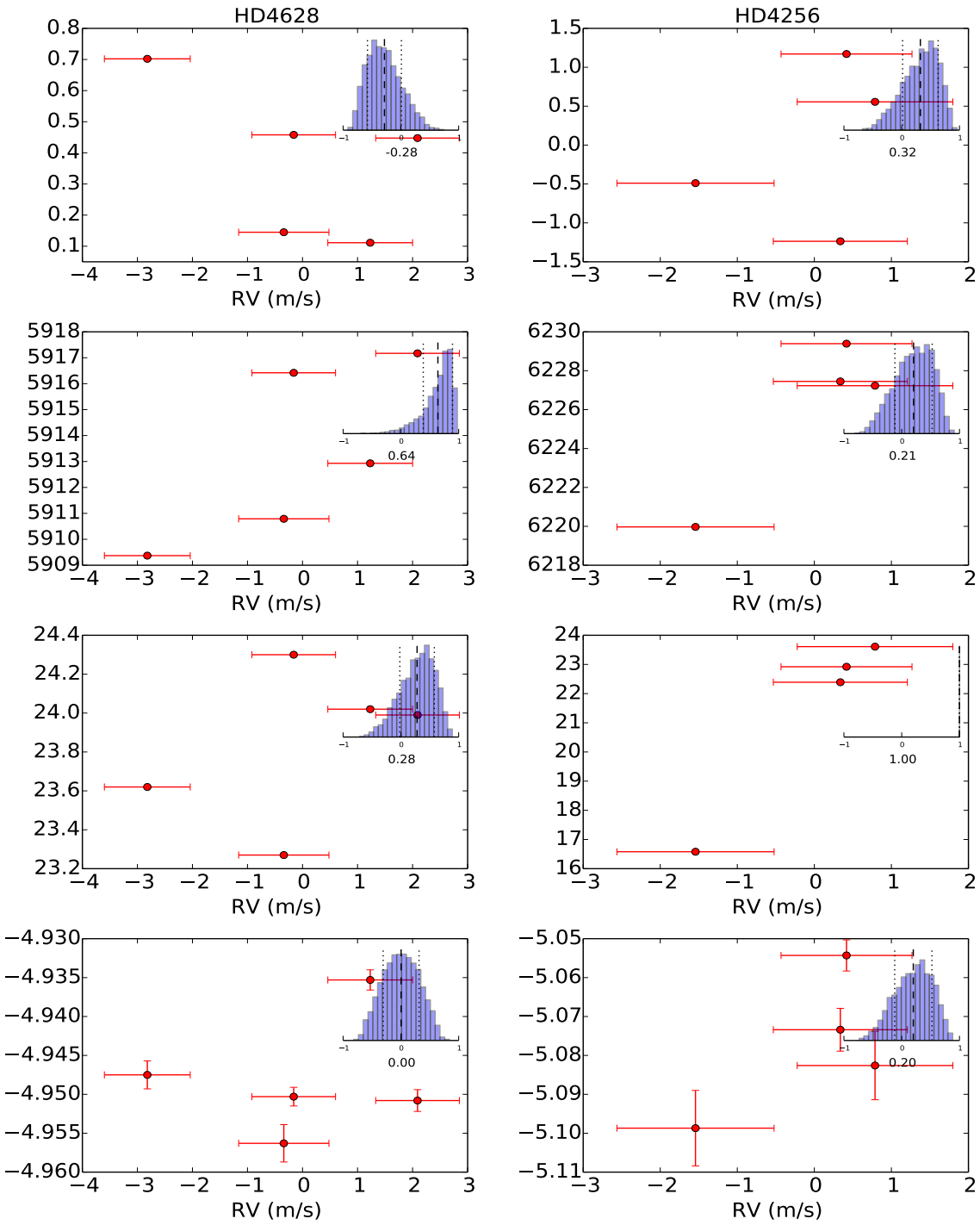

Fig. B.1. continued.